Article

Optimization of a Novel Urban Growth Simulation Model Integrating an Artificial Fish Swarm Algorithm and Cellular Automata for a Smart City

Xinxin Huang [1],*, Gang Xu [2] and Fengtao Xiao [3]

1 School of Resource and Environmental Science, Wuhan University, 129 Luoyu Road, Wuhan 430079, China
2 School of Remote Sensing and Information Engineering, Wuhan University, 129 Luoyu Road, Wuhan 430079, China; xugang@whu.edu.cn
3 Wuhan Urban Construction Group, 9 Changqing Road, Wuhan 430022, China; fengtao-xiao@whu.edu.cn
* Correspondence: huangxin2015@whu.edu.cn

Abstract: As one of the 17 Sustainable Development Goals, it is sensible to analysis historical urban land use characteristics and project the potentials of urban sustainable development for a smart city. The cellular automaton (CA) model is the widely applied in simulating urban growth, but the optimum parameters of variables driving urban growth in the model remains to be continued to improve. We propose a novel model integrating an artificial fish swarm algorithm (AFSA) and CA for optimizing parameters of variables in the urban growth model and make a comparison between AFSA-CA and other five models, which is used to study a 40-year urban land growth of Wuhan. We found that the urban growth types from 1995 to 2015 appeared relatively consistent, mainly including infilling, edge-expansion and distant-leap types in Wuhan, which a certain range of urban land growth on the periphery of the central area. Additionally, although the genetic algorithms (GA)-CA model and the AFSA-CA model among the six models due to the distance variables, the parameter value of the GA-CA model is −15.5409 according to the fact that the population (POP) variable should be positively. As a result, the AFSA-CA model regardless of the initial parameter setting is superior to the GA-CA model and the GA-CA model is superior to all the other models. Finally, it is projected that the potentials of urban growth in Wuhan for 2025 and 2035 under three scenarios (natural urban land growth without any restrictions (NULG), sustainable urban land growth with cropland protection and ecological security (SULG), and economic urban land growth with sustainable development and economic development in the core area (EULG)) focus mainly on existing urban land and some new town centers based on AFSA-CA urban growth simulation model. An increasingly precise simulation can determine the potential increase area and quantity of urban land, providing a basis to judge the layout of urban land use for urban planners.

Keywords: an artificial fish swarm algorithm; machine learning; optimization; landscape indicators; scenario simulation; sustainable urban development

1. Introduction

More than 56% of dwellers now from four corners of the globe resided in urban areas, with increasing number of inhabitants reaching to 68% by 2050. China will see an astonishing increase to 80% of the urban population in 2050 [1]. Due to the rapid flow of people into urban areas across the past decades, the speed of urbanization is projected to continue [2]. As a result, various problems, such as traffic congestion, landscape fragmentation, and global warming, follow close on another [3–5]. Although the impact of all these problems should not be contributed to human activities, some of them are partly addressed by human's behaviors. Henceforth, authorities and citizens across the world together have taken action to regulate urban growth patterns. In the highly competitive urban areas, the right spatial layout of limited land resources will be an effective means to

reduce the influence of urban land growth. However, this spatial layout of urban growth is unlikely to rely on a supply of maps and labors resembling the conditions in the last decades because the competition is stiff and the technology develops fast. The smart city is not just analyzing the urban development characteristics and human behaviors but assisting with technology [6]. The improvements of technology applying in urban simulation process allow us to study the potential trend and make various projections of urban growth for consequent generations. With the aid of these technologies, it is easier for relevant researchers to explore the spatial change trend of urban area and seek valid planning alternatives for the sustainable development in cities.

The cellular automaton (CA) simulation model, which is a bottom-up and discrete model with a series of cells, is the most widely used for projection of urban growth and estimate the impact of urbanization [7,8]. At the global scale, Professor Li and his team presented a fine spatial resolution of 1 km to project possible urban growth under shared socioeconomic pathways in the Yangtze River Delta region, USA, and other representative countries [9]. It is projected that the highest figure for these zones in the newly urban land from current cropland by 2100 will reach to around 63%. At the local scale, to tackle the problems between urbanization, such as land use, land planning policies, and the unparalleled economic process, Yang et.al predicted the future land use patterns by 2030 in the Beijing–Tianjin–Hebei, before studying historical land use characteristics in the past 15 years, with a combination of CA model and other effective models [10]. Taking into government agent and residents agents, Xu et.al conquered the limitation of the impact of human activities on urban growth cells to achieve the goal of learning heterogeneity in various interactions [8]. However, the CA model is partly limited by the impact of spatial variables closely related to urban growth, especially the weight parameter corresponding to each spatial variable affecting directly the simulation accuracy [11].

It is necessary to reduce inaccurate and time-consuming possibilities in the subjective determination process of the weight parameters of these variables [11]. Wu and Webster [12] used binary logistic regression (BLR) to obtain the parameters in the CA model. This method optimizes the smallest gap by calculating the difference between the simulated result and the actual result. However, BLR is suitable for linear relationships, and changes in urban land use and variables are non-linear [11]. Subsequently, many machine learning methods have been combined with CA models, such as evolutionary algorithms (e.g., genetic algorithms (GAs)), swarm intelligence methods (e.g., ant colony algorithms (ACOs) [13]), the particle swarm optimization (PSO) algorithm [14], *biogeography*-based *optimization* (BBO) [15]), artificial neural networks [16], and support vector machine [17]. However, artificial neural networks work as "black boxes", which is not conductive to the interpretation of the principle [11,18]. PSO is mainly used for continuous problems, and may fall into local optima, whereas the ACO algorithm has certain requirements for the parameters, and is slow to converge [19]. The BBO optimization unconstrained problem can obtain good optimization results, but because the traditional gene transfer method is less efficient in obtaining information, it can only use the existing information of the population [20]. GA selects individuals through crossover and mutation, but the selection probability of crossover and mutation directly affects the convergence of the algorithm [21].

The artificial fish swarm algorithm (AFSA) is one of the most advanced swarm intelligence algorithms [22]. This algorithm is a behavior-based algorithm that was inspired by the social behaviors of fish, and it combines artificial intelligence technology with biology [23,24]. The AFSA algorithm has the characteristics of a fast convergence speed, insensitivity to the initial values, strong adaptability, and strong fault tolerance [25]. As a result, it is better able to optimize non-linear functions in complex environments. In addition, the strong fault tolerance helps it to jump out of locally optimal solutions. Therefore, when the AFSA algorithm is applied to global optimization, it has distinct advantages over the other algorithms [26,27]. It has also been used in many different applications, including engineering problems [28–30], biological problems [25], and trial and error detection [31]. Liu et.al detected the weak character signal by optimizing the system parameters with

AFSA [32]. Zhao et.al identified true flaws without any prior knowledge about structures integrating AFSA and the artificial bee colony [29], while AFSA is used to solve large-scale reliability-redundancy allocation problem [33], and it is applied to solve the o–1 multidimensional knapsack problem in the study of Md. Abul Kalam Azad et al. [30]. To date, although the AFSA algorithm has been applied in many different fields, to the best of our knowledge, it has not been used in urban growth research.

Sustainable development is to satisfy the needs of current people without doing harm to the future generation's lives. Wuhan is an important part of the regional urban development system of China. It is the largest transportation network hub in China, and plays a crucial role in shaping the national agricultural strategy. With the potentials of urban growth simulation, it is easier to analyze the historical characteristics of urban areas and provide the spatial planning references on urban areas through quantitative analysis and the efficient technology [34]. Henceforth, the contributions of our study may be multiple. Firstly, the urban land in the study area was spatially linked to various urban growth-related variables. The traffic road variable was calculated by the Euclidean distance to obtain raster data. The AFSA algorithm and five other comparison methods were used to obtain the weight features of all the variables. BLR was applied to establish the relationship between the urban land-use change and a set of related variables. The weight parameters of the AFSA, ACO, BBO, PSO, and GA algorithms were then optimized in the MATLAB environment. Once the urban cell conversion probability was calculated, the various integrated CA models were then used to simulate the urban growth changes from 2005 to 2015 in Wuhan. Finally, after the model assessment, the urban land use for 2025 and 2035 was predicted by the integrated urban growth models. The main intention of this study is to propose a possible solution for urban growth simulation: (1) to determine the weight parameters of driving variables about urban growth, (2) to explore the characteristics of historical urban growth patterns in local scale, and (3) to provide potential projections under three simulation scenarios with relatively reasonable urban growth simulation model (approximately 20 years).

2. Case Study Area and Data

2.1. Study Area

Wuhan, the capital city of Hubei province in China, has an area of about 8494.41 km^2 (Figure 1). With one of the largest transportation network hubs in China, Wuhan plays a key role in shaping national agricultural strategy. Wuhan's urban development has followed the growth modes of axis development, ring filling, and annular layer expansion (Chen et al., 2019). In early 2019, Wuhan issued a new urban plan for the time period of 2017 to 2035. According to the new plan, the entire city of Wuhan is divided into four groups: the central activity area; the deputy city centers; the new city centers; and the town center areas, which are represented using different shapes and colors in Figure 1. The city's three rings divide the city into the following areas: the central activity area, the deputy city centers (which include Jianghan Bay, Sixin, Nanhu, Luxiang, Yangchunhu, Songjiagang, Wuhu, Yujiji, Zhuankou, and Leopard), and other areas. The group/town centers are the sub-districts or townships. Based on the new plan, Wuhan will not be a traditional urban city, as most sites will be unique areas, such as Jiangxia, Wulijie, and Cangjie. There is also a growing inconsistency between urban land use and cultivated land protection in Wuhan. Hence, it is crucial to improve the urban economic development of Wuhan by optimizing the allocation of land resources.
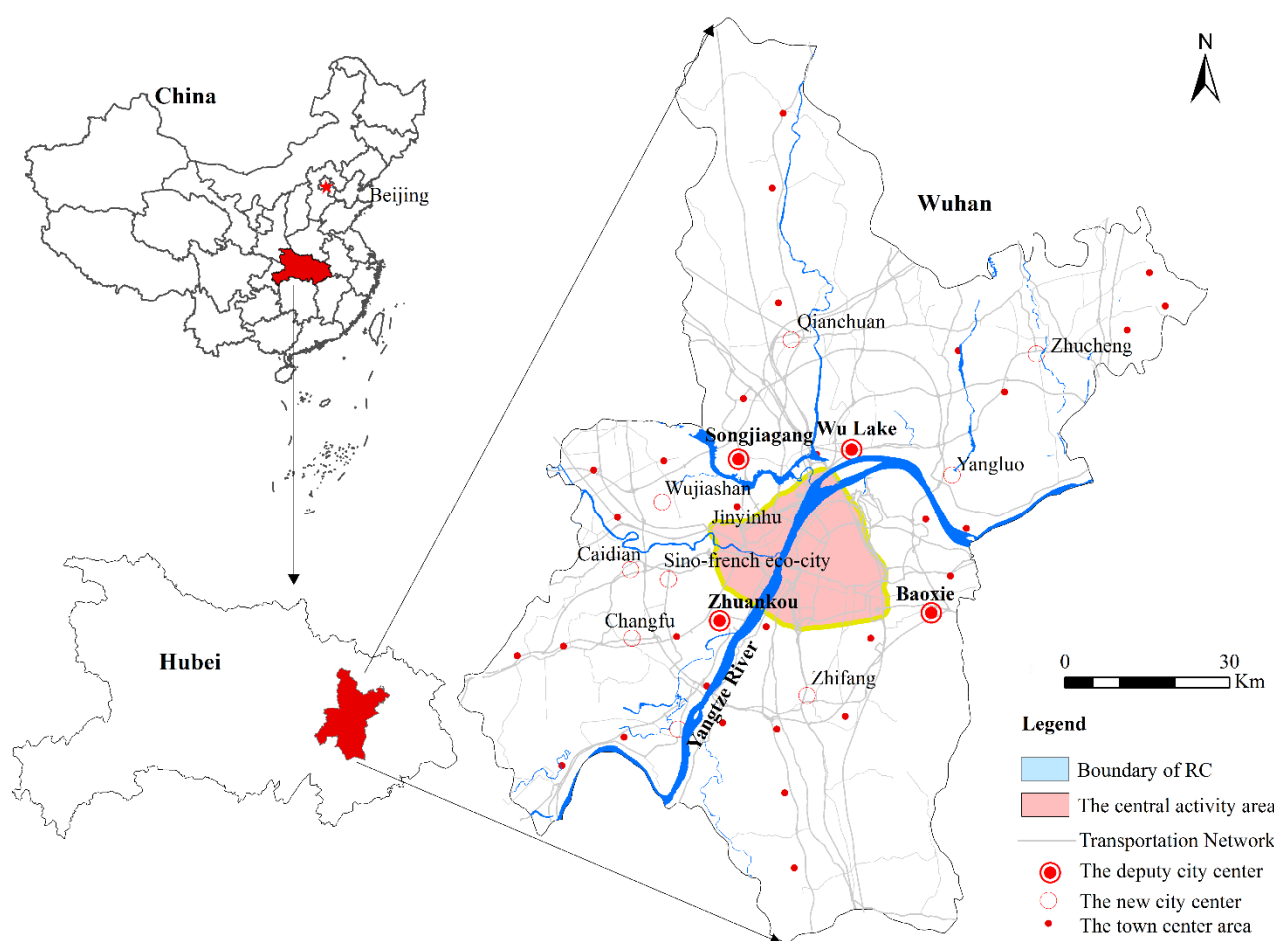
Figure 1. Study area.

2.2. Data Acquisitions

The data used in this study can be roughly divided into two categories: land-use data and auxiliary data (Table 1). A span of ten years can reveal comprehensively the historical characteristics of urban growth and the reasonable potentials of future urban areas. The first two periods are used to determine the weights of variables, and the last one is for optimizing the model. The land-use datasets (1995, 2005, and 2015) were obtained from the Data Centre for Resources and Environmental Sciences at the Chinese Academy of Sciences (http://www.resdc.cn/data.aspx?DATAID, accessed on 18 January 2021). The accuracies of these datasets are 92.90%, 94.30%, and 93.00%, respectively [35], and the spatial resolution is 30 × 30 m. The remote sensing interpretation of the land use was mainly based on Landsat Thematic Mapper /Enhanced Thematic Mapper Plus and Landsat 8 remote sensing data. The data projection system was the Albers equal-area Conic projection. The south standard parallel was 25° N, the north standard parallel was 47° N, and the central longitude was 105° E. The origin of the coordinates was the intersection of the central longitude and the equator. In line with the aim of this study, we extracted data from the designated regions and reclassified the data into three categories on the basis of the land-cover use: urban, non-urban, and water.

Table 1. The response and explanatory variables used in this study.

Dataset	Type	Year	Full Meaning	Acquisition Method	Purpose
LUD$_1$	GRID	1995	Land-use in 1995	Reclassification	To create the land-use patterns
LUD$_2$	GRID	2000	Land-use in 2000	Reclassification	To create the land-use patterns
LUD$_3$	GRID	2015	Land-use in 2015	Reclassification	To create the land-use patterns
D-nat	Shpfile	2015	Distance to national road	Euclidean distance	Global driving factor
D-hig	Shpfile	2015	Distance to highway	Euclidean distance	Global driving factor
D-pro	Shpfile	2015	Distance to provincial road	Euclidean distance	Global driving factor
D-rai	Shpfile	2015	Distance to railway	Euclidean distance	Global driving factor
D-cou	Shpfile	2015	Distance to country road	Euclidean distance	Global driving factor
POP	GRID	2015	Population	Resample	Global driving factor
DEM	GRID	2015	Digital elevation model	Resample	Global driving factor
GDP	GRID	2015	Gross domestic product	Resample	Global driving factor
NEI	GRID	-	Neighhood cell	-	Local driving factors

It is not necessary for urban land models to include all the relevant factors, especially in the case of non-sensitive factors [36]. Considering the natural and economic situation in Wuhan, the transportation network, population (POP), digital elevation model (DEM), and gross domestic product (GDP) were selected as the auxiliary data in this study. The auxiliary data were traffic data (distance to roads), natural attribute data (e.g., DEM), social attribute data (e.g., GDP and POP), and planning data. The distance to different levels of road and the DEM data were obtained from the Geospatial Data Cloud Platform (http://www.gscloud.cn/sources/accessdata/310?pid, accessed on 18 January 2021), then we used the Euclidean distance to calculate the spatial distance. GDP and POP data were also obtained from RESDC (http://www.resdc.cn/data.aspx?DATAID, accessed on 18 January 2021). The time span of these factors was the year of 2015. The planning data were extracted from the urban master planning map (2015–2030 and 2018–2035) produced by the City Planning Office of Wuhan.

3. Methodology

In this study, we developed a novel combined model (AFSA-CA) to simulate urban growth. As shown in Figure 2, the proposed model includes the following main steps:

(1) Preparation of training data: the land-use data are reclassified and divided into urban land, non-urban land, and water. Each variable is then associated with each grid cell in the study area, and the Euclidean distance is used to calculate the distance to each level of road.

(2) Optimized the parameter of each variable: In the MATLAB R2014 a software environment, the acquired data samples are used to obtain the weight of each variable by the six methods (BLR-CA, ACO-CA-CA, BBO-CA, PSO-CA, GA-CA, and AFSA-CA).

(3) Calibrating CA models for urban growth land simulation: the conversion probabilities acquired by the six methods are applied to calibrate the urban land expansion model with the cell neighborhoods, the constraint coefficients, and random factors.

(4) Accuracy assessment: The performance of the calibrated models is evaluated using a visual comparison, the Kappa coefficient, and the figure of merit (FoM), and landscape indicators.

(5) Future scenario simulation: the proposed model (AFSA-CA) is applied to simulate the urban land growth in 2025 and 2035 under different scenarios.
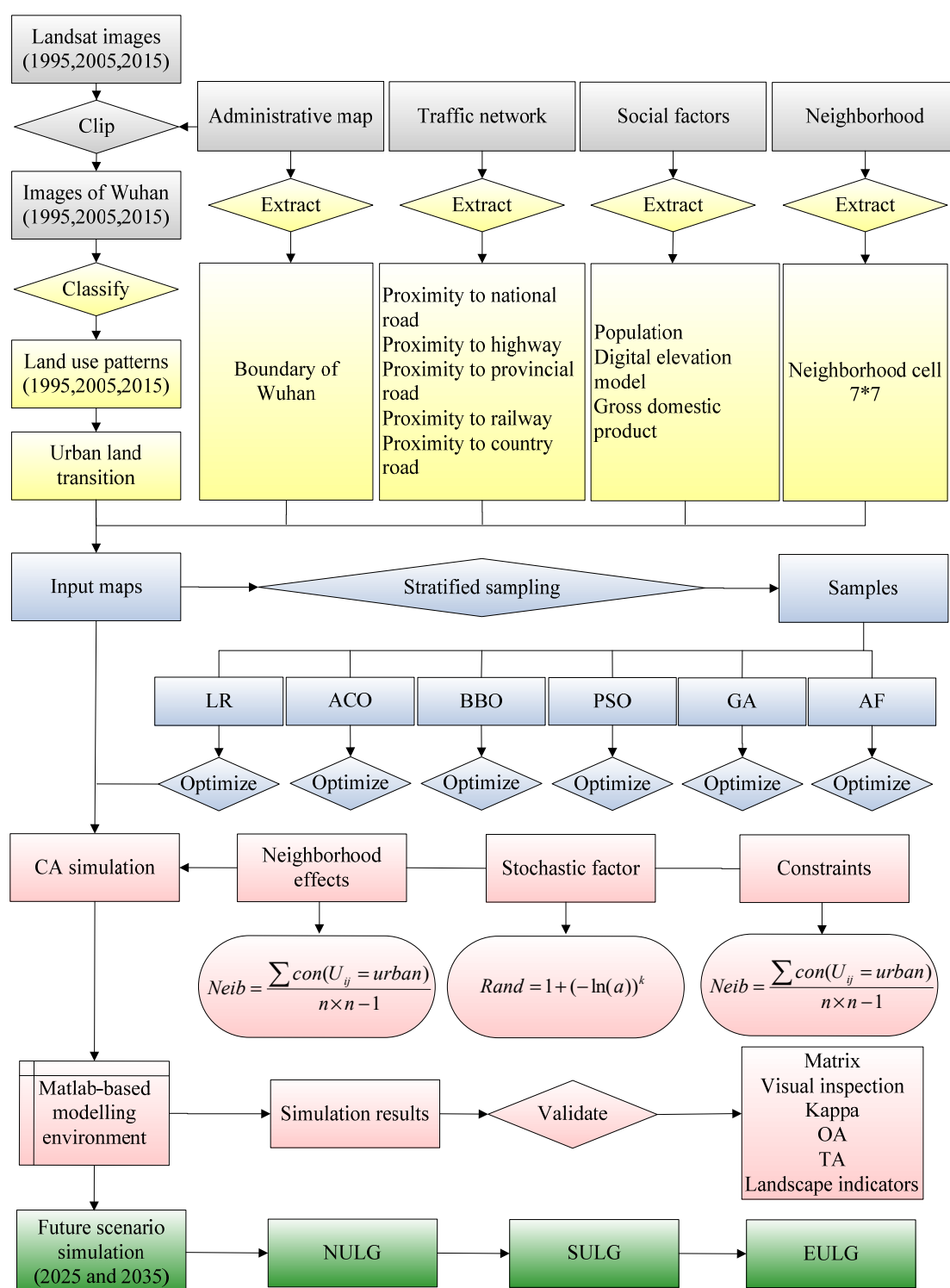
Figure 2. Flowchart of the methodology for the simulation of the urban land-use changes.

3.1. The Urban CA Model

The urban CA model is composed of unit space, unit, unit state, neighborhood, conversion rule, and time. The acquisition of conversion rules is the core of the urban CA model [37]. In the simulation of urban land use growth, the conversion probability of a cell can be determined by a multi-criteria judgment method based on a series of factors. Since these factors and the development of land cells do not meet the conditions of normal

distribution, we can use logistic regression technology to modify the urban CA model [38]. The conversion probability of the study area is summarized by the following formula:

$$P_g(s_{ij} = urban) = \left(1 + \sum_i^n (-(a_0 + \omega_i x_i))\right)^{-1} \tag{1}$$

In the formula, P_g is the global transformation probability, S_{ij} is the state of the cell, a_0 is a constant, x_i is a series of influence factors, and ω_i is the weight corresponding to each factor.

Considering the spatial compactness, urban planning, and subjective constraints, etc., neighborhoods (*Neib*), constraints (*Suit*), and random factors (*Rand*) are usually added to the urban CA model. *Neib* means that the central cell is affected by other surrounding cells, which can be expressed as:

$$Neib = \frac{\sum con(U_{ij} = urban)}{n \times n - 1} \tag{2}$$

In the formula, *con ()* is a conditional function, assuming U_{ij} is a city cell, then *con ()* returns 1; if U_{ij} is a non-urban cell, *con ()* returns 0.

Suit represents the constraint conditions in the urban land growth simulation, which can be expressed as:

$$Suit = con(T_{ij} \neq water) \tag{3}$$

In the formula, T_{ij} represents the land use type of the cell. If T_{ij} is a water area, *con ()* returns 0; otherwise, it returns 1.

Rand represents the random interference function, used in the urban CA model to reflect the uncertainty of urban land use changes, which can be expressed as:

$$Rand = 1 + (-\ln(a))^k \tag{4}$$

In the formula, *a* is a random number of [0,1], and k is a parameter that controls the degree of influence of a, and the value is an integer of [1,10].

In summary, the transformation probability P_g, the neighborhood constraint *Neib*, the constraint factor *Suit* and the random variable *Rand* are multiplied to modify P_g, which can be expressed as:

$$P_g = \left(1 + \sum_i^n (-(a_0 + \omega_i x_i))\right)^{-1} \times Neib \times Suit \times Rand \tag{5}$$

Set the threshold P_{thre} for transforming non-urban cells into urban cells, and compare P_g with the magnitude to determine the state of U_{ij} at t + 1. When $P_g > P_{thre}$, U_{ij} is transformed into a city cell, otherwise, U_{ij} keeps the original state of the cell.

The simulation process for each cell can be summarized as follows: the cell can only change if it conforms to the development probability. The simulation period in this study was divided in two phases: calibration of the model for 2005–2015, and simulation of the future land use.

3.2. Six Optimization Methods

In Section 3.1, a series of factors have different effects on urban cell transformation. Here, we call the degree of this effect the weight parameter of each factor. A cost function is usually designed for solving optimization problems. Mathematical or intelligent methods

are then applied to obtain the parameters that minimize the objective function. The function can be depicted as:

$$\begin{cases} f(x) = \sum_{i}^{n} (f_{ai} - f_{si})^2 \\ f_{si} = \left(1 + \sum_{i}^{n} \left(-(a_0 + \omega_i x_i) \right) \right)^{-1} \end{cases} \tag{6}$$

where $f(x)$ represents the objective function (Equation (1)); f_{ai} and f_{si} represent the actual land-use state and the simulated land-use state, respectively, which is made up of the urban land state (1) and non-urban land state (0); a_0 is a constant; and ω_i is the weight of factor x_i.

We propose a new algorithm, artificial fish school algorithm, to obtain the optimal parameter combination of influencing factors, and construct AFSA-CA. The BLR and other intelligent algorithms with the optimized CA model are compared with it (Figure 2).

3.2.1. AFSA Optimization Process

The AFSA algorithm is inspired by the natural behavior of fish populations, and applied to solve similar optimization problems [39]. For optimization problems, the food concentration optimization variable around an artificial fish corresponds to a parameter solution set. Assuming that there are m spatial variables corresponding to the parameters of $m + 1$ spatial variable, the dimension of the food concentration is $m + 1$; the optimal value of food concentration indicates the pros and cons of the solution.

It has powerful search capabilities, is not prone to falling into local optima, and helps to achieve global optimality. It also features a robust design, simple operation, and flexibility of use [39]. Through continuous learning and repeated trials of the selected models, the field of view of the artificial fish and the step size (Equation (7)) are dynamically adjusted to speed up the search and improve the balance between the global and local search capabilities, in addition to generating search points to find a better location.

$$\text{Step} = Step_{\max} - (Step_{\max} - Step_{\min}) * Step / MAXGEN$$

$$Vision = Vision_{\max} - (vision_{\max} - vision_{\min}) \cdot step / MAXGEN \tag{7}$$

The vision parameter is equal to the visual range of AFSA, and v_i is the position where AFSA wants to move in the visual range. If v_i has a better environment than the current position v, it goes without saying that AFSA moves toward v_i. $Dist_{v-vi}$ represents the distance moved and is calculated from the Euclidean distance (Equation (3)).

$$Dist_{v-vi} = \sqrt[2]{\sum_{d=1}^{D} (v - vi)^2} \tag{8}$$

At the end of each iteration of executing the AFSA algorithm, the vision value is updated. Xiaolei et al. (2002) found that when the step size of AFSA is set as a larger value, and the larger the vision parameter value, the faster the convergence, but after convergence, it is necessary to search for a better position to avoid local search. If the vision value is set as a smaller value, the convergence speed drops sharply. Therefore, the dynamic vision and step values should be set to fit the global search.

In order to solve the problem of determining the maximum value, the AFSA algorithm uses the idea of collective cooperation, i.e., the higher the physical concentration of artificial fish, the closer the value for the artificial fish will be to the optimal solution. Figure 3 is used to describe the process of determining the solution domain, where G_1 is the global optimal solution, L_1 is the constrained optimal solution, and Y represents the set of global optimal solutions. On this basis, it is possible to find a more accurate global optimal solution for the solution field. In fact, the center of gravity is usually considered to be the global optimal solution in the range of the solution domain.
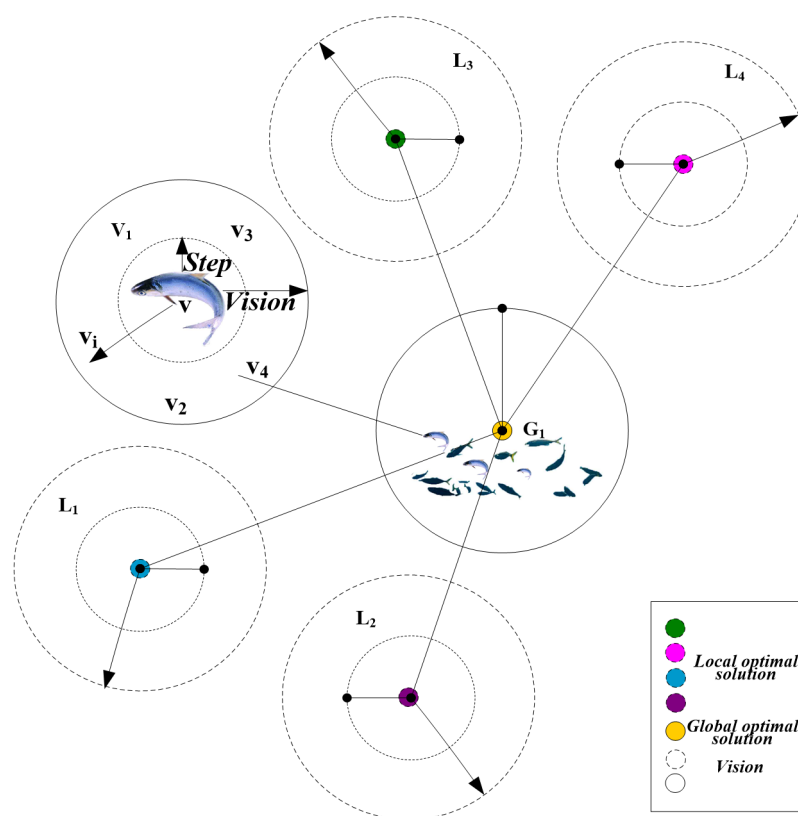
Figure 3. Determining the solution domain.

The behavior of the artificial fish is divided into four groups: clustering, randomization, chasing, and foraging. The best position is then determined by evaluating the values obtained by analyzing these behaviors. As in the other intelligent bionic algorithms, the AFSA algorithm first initializes the parameters and randomly generates initial values. The parameters of the AFSA algorithm include the total number of artificial fish, the try number, the number of iterations, the maximum number of iterations, the move step of the artificial fish, the crowding factor, and the field of view (Table 2).

Table 2. Algorithm parameter set.

Set Parameters	Expression Form	Significance
Total number	N	A set of candidate solutions
Try_number	Try_number	Maximum number of heuristics per move
Iterations	NC	Number of repetitions
Max-iterations	NC_max	Maximum number of repetitions
The artificial fish movement distance	$step$	Distance of each step
Crowding factor	δ	Judgment on merits of the environment
Field of view	$vision$	Range of vision

Through the neighborhood search, the relevant information is obtained to determine the best information. If, through evaluation, it is found that the searched information is better than the information displayed on the bulletin board, the bulletin board is updated to achieve optimization; otherwise, the search continues. The entire process of the AFSA algorithm is shown in Figure 4.
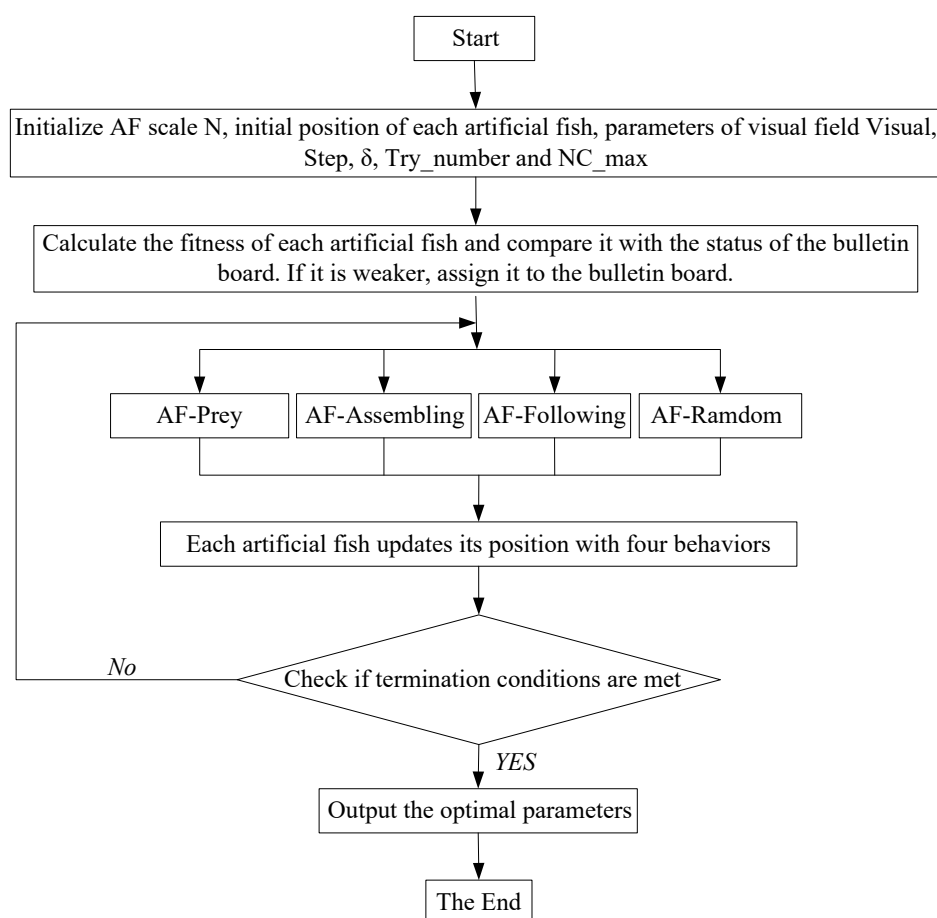
Figure 4. Flowchart of the artificial fish swarm algorithm (AFSA) algorithm.

The following are the behaviors of artificial fish:

(1)   AF-Prey

AF-Prey denotes the most basic behavior of living creatures. Since the basic behavior of artificial fish is foraging, the algorithm functions by observing the winding process close to a food site in water. This is done by pinpointing the high concentrations of fish in the water, determined by their direction of swimming, which in turn signals a high food concentration.

$$X_j = X_i + Visual \cdot Rand\,() \tag{9}$$

In formula (9), X_i is the information regarding the current position of an artificial fish. Within a certain range of perception, the artificial fish randomly selects their next point and obtains another position X_j. To better simulate randomness, the *Rand ()* function is added, with a value range from 0 to 1. Since the maximum and minimum values can be interchanged in function optimization problems via functions such as inverse, the choice of maximum and minimum values is dependent on the actual problem. If the value to be optimized is a maximum value, i.e., $Y_i < Y_j$, the artificial fish moves one step toward the randomly selected direction. The mathematical expression is illustrated as follows:

$$X_i^{t+1} = X_i^t + \frac{X_j - X_i^t}{\|X_j - X_i^t\|} \cdot Step \cdot Rand\,() \tag{10}$$

Conversely, if the value that needs to be optimized is a minimum value, i.e., $Y_i > Y_j$, the artificial fish moves a step forward. If the above-stated conditions are not satisfied, it is necessary to randomly select the state of the resulting movement to predict the future movement. If the conditions for actualizing forward motion are still not obtained after

many attempts, a random direction can be chosen to affect forward movement. The function equation for random movement is as follows:

$$X_i^{t+1} = X_i^t + Visual \cdot Rand\,() \tag{11}$$

(2) AF-Assembling

Fish generally select their swimming direction based on the behavior of other fish. Swimming in groups, which is called aggregation behavior, is not only convenient for foraging, but also offers protection against predators. In the case of fish, the fish group does not require a leading fish as the fish choose their surroundings based on each other's relative motion.

This behavior of fish groups for foraging and protection maintains their survival. Therefore, as an algorithm, every fish should move as close as possible to the center of their surroundings and avoid crowding. This can be described, mathematically, as follows:

$$X_i^{t+1} = X_i^t + \frac{X_c - X_i^t}{\|X_c - X_i^t\|} \cdot Step \cdot Rand\,() \tag{12}$$

where X_i denotes the current position information of the artificial fish. When $d_{ij} < vision$, the surrounding neighborhood of the artificial fish is searched. When the average concentration of central food in the neighborhood is greater than the average concentration of food in the neighborhood where the artificial fish are located, the location is considered to be optimal, and the artificial fish are then moved to the new central position; otherwise, they feed directly.

(3) AF-Following

Fish ascertain their movement based on the swimming direction of other fish; when they receive information about a better location with more food, they quickly follow the fish or fish group to reach the new location. In rear-end behavior, each artificial fish moves toward a position of higher value, followed by the fish or fish group. This behavior is used in the optimization algorithm, and can be calculated as follows:

$$X_i^{t+1} = X_i^t + \frac{X_j - X_i^t}{\|X_j - X_i^t\|} \cdot Step \cdot Rand\,() \tag{13}$$

where X_i is the current positional information of an artificial fish. When $d_{ij} < vision$, the surrounding neighborhood of the artificial fish is searched. When the average concentration of central food in the neighborhood is found to be greater than the average concentration of food in the neighborhood where the artificial fish are located, the new position is considered to be better, prompting movement of the artificial fish to this central position; otherwise, they feed directly.

(4) AF-Random

It is unique to see fish swimming freely in the water, which is manifested in the form of a haphazard swimming direction. In essence, this random behavior of fish is aimed at enlarging the scope of their field of search, to reach a position with greater food concentration.

This random behavior of fish is to find optimal solutions in a fast way, i.e., the range of the fish's vision is adjusted, a state is randomly selected, and the fish swims in that direction. However, this random foraging behavior is usually not rigorous. The pseudo-code of the AFSA algorithm is shown in Table 3.

Table 3. The pseudo-code of the artificial fish (AF) algorithm is given in Algorithm AF.

Algorithm 1: The Pseudo-code of the AF Algorithm
Procedure the initial artificial fish swarm
Set gen = 1
While gen <= MAXgen
Print the food consistency and positions for fishes
Assess the print result
Calculate the behavior
Float AF-prey
Float AF-follow
Float AF-swarm
Float AF-random
If the maximum of the dependent > the best of the gen
Produce the best solution
And if
Define the best solution
Record current best solution
Gen = gen + 1
End repeat

3.2.2. Five Optimization Methods for Comparison

BLR is an empirical technique utilized for modeling urban growth where binary values are dependent and independent in the SPSS software. BLR can be used to easily establish the contribution of every urbanization driving force as an independent variable [40]. The dependent variable takes the value of 1 (changed cell) or 0 (non-changed cell), and is estimated as shown in the following formula:

$$BLR = \exp(a_0 + a_i * x_i) / (1 + \exp(a_0 + a_i * x_i)) \tag{14}$$

However, since the study of urban dynamics needs to consider both the spatial and local characteristics of the independent variables, *BLR* is a static model with serious defects [11]. However, we can take this traditional method as a base comparison.

These swarm intelligence optimization algorithms (ACO, BBO, PSO, and AFSA) are among efficient optimization algorithms. To achieve the optimal optimization results, it is sensible to simulate complex, intelligent swarm behaviors between simple animal individuals, such as their information interactions and collaborations. Although the design ideas of these algorithms are different, and the performance and application fields have some limitations, these algorithms generally have some commonalities.

(1) Animals tend to form small social groups. Thus, individuals need to rely on the power of group cooperation to survive and perform activities.

(2) In terms of information exchange, social groups survive through information exchange. The ACO algorithm interacts with the information of pheromones, while the PSO and AFSA algorithms directly interact with the current position information.

(3) Positive feedback is required, and effective suppression is also required. For example, the ACO algorithm relies on the pheromone evaporation mechanism and AFSA introduces a "crowding" factor.

(4) The algorithms avoid falling into local extrema and introduce random factors. For example, the ACO algorithm selects paths randomly, a random number is used in PSO, and random steps are used in AFSA.

For the comparison, the intelligent algorithms were calibrated using the same samples. The basic principle of ACO is to find the path by randomly selecting attribute nodes. Due to this kind of random selection of attribute nodes, it is a relatively time-consuming process. Therefore, a heuristic function is introduced into the search process to save search time.

The BBO algorithm is an optimization algorithm based on biological population, which was proposed by Simon in 2008 [41]. The living environment of each biological

species contains characteristic variables, such as temperature, precipitation, and landform, which jointly determine the capacity of this habitat. Habitat capacity is usually expressed in terms of a fitness index. The higher the fitness index, the more population the habitat contains. Two indicators that directly reflect habitat fitness are the immigration rate and out-migration rate. This species migration model is shown in Figure 5.
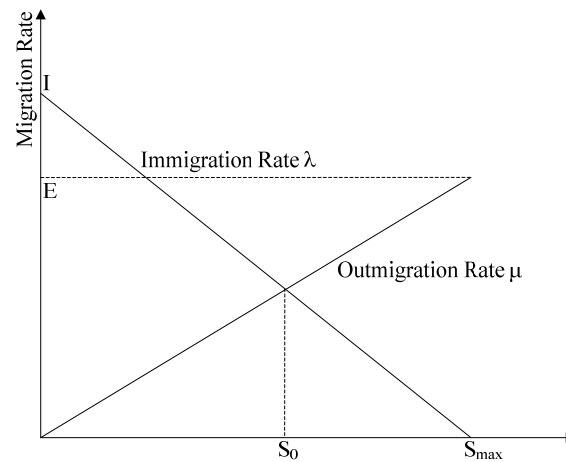

Figure 5. The species migration model.

As can be seen in Figure 5, the immigration rate is decreasing and the out-migration rate is increasing. Assuming that the probability of S is Ps, then the probability of P being in the time range from T to Δt is denoted as

$$P_{\mathrm{s}} = \begin{cases} P_{\mathrm{s}+1}\mu_{s+1} - P_{\mathrm{s}}(\lambda_s + \mu_s) \\ P_{\mathrm{s}-1}\mu_{s-1} + P_{\mathrm{s}+1}\mu_{s+1} - P_{\mathrm{s}}(\lambda_s + \mu_s) \\ P_{\mathrm{s}-1}\mu_{s-1} - P_{\mathrm{s}}(\lambda_s + \mu_s) \end{cases} \tag{15}$$

When the species population number reaches S_{max}, $P = [P_0, P_1, \cdots, P_N]^T$, then P can continue to be expressed as follows:

$$A = \begin{bmatrix} -(\lambda_0 + \mu_0) & \mu_1 & 0 & \cdots & 0 \\ \lambda_0 & -(\lambda_1 + \mu_1) & \mu_2 & \ddots & \vdots \\ \vdots & \ddots & \ddots & \ddots & \vdots \\ \vdots & \ddots & \lambda_{n-2} & \lambda_0 & \mu_n \\ 0 & \cdots & 0 & \lambda_{n-1} & -(\lambda_n + \mu_n) \end{bmatrix} \tag{16}$$

The difference between the PSO and ACO algorithms is that the flying space of birds requires not only a range of vision, but also the movement speed, to determine the probability of getting food. The basic principle of the ACO algorithm is that there are n particles in a group searching in a certain space S, where each particle records its original position and flight speed. When the search reaches the optimal solution, it compares this with the other optimal solutions in the group, and updates its position in time to obtain the global optimal solution. Generally speaking, the position and velocity functions of particles are expressed as follows:

$$v_i = \omega \cdot v_{i0} + c_1 \cdot rand\,() \cdot (l_i - x_{i0}) + c_2 \cdot rand\,() \cdot (G_i - x_{i0}) \tag{17}$$

$$x_i = x_{i0} + v_i \tag{18}$$

where w represents the inertia value; v_{i0}, v_i represent the initial speed and the running speed of the particles; x_{io} and x_i represent the initial position and the position of the particles; and

l_i and G_i represent the local and global optimal solutions. C_1 and C_2 represent the learning factors and are usually between 0 and 2. *Rand ()* represents a random number, which is usually between 0 and 1.

The concept of GAs was first developed by Holland in 1960, following the original evolutionary process of "survival of the fittest" and "natural selection" [42]. GAs consist of two important steps: crossover and mutation. Crossover retains the best chromosome of each individual, while mutation creates mutated offspring.

All of these algorithms can be applied to optimize the variable of model urban growth model, as relatively good alternatives to traditional search [31,43]. Beginning with the initial population of each grid cell, the process is run for 50 generations, to search for better rules for each grid cell, in order to define the parameters of the variables and the constant values. In this study, the obtained rules for 2005 could then be used to predict the values for 2015. The same rules could also then be applied to simulate the future values for 2025 and 2035.

3.3. Accuracy Assessment

The six optimization methods are to calibrate CA model under the same data background (land use data and variable data) and equipment environment. The simulation assessment of CA models needs robust proof (Jenerette and Wu, 2001). Visual inspection is one way to compare the actual and simulated areas (Ward et al., 2000). In this study, we also validated the agreement of the CA models using statistical methods, including the Kappa coefficient, FoM [44], urban accuracy (UA), and total accuracy (TA). The range of the Kappa coefficient is from 0 to 1, with a higher value representing stronger agreement (McHugh, 2012). The FoM value contains three indices: hits, misses, and false alarms. The hits indicate correctly forecast urban growth cells; misses represent actual urban growth cells that are missing in the simulation; and false alarms indicate disagreement between the actual and simulated cells. UA and TA are point-to-point checks. The formulas for the statistical measures are as follows:

$$Kappa = (P_0 - P_c)(1 - P_c) \tag{19}$$

$$P_c = \frac{(a_1 \times b_1 + a_2 \times b_2)}{n^2} \tag{20}$$

where P_0 is the ratio of the number of correctly simulated grid cells to the total number of grid cells, and Pc is the ideal consistency. a_1 and b_1 denote the actual and simulated urban cells, respectively. Similarly, a_2 and b_2 represent the actual and simulated non-urban cells, respectively.

$$FoM = \frac{Hits}{Hits + Misses + FalseAlarms} \tag{21}$$

where "Hits" are the number of actual or simulated urban cells; "Misses" are simulated as non-urban cells; and "FalseAlarms" are simulated as urban cells, but are not in fact actual urban cells.

Landscape indicators can measure the spatial urban form [11,45]. We choose three landscape indicators to measure the form of urban growth: the number of urban patches (NP), average perimeter ratio (PARA_MN) and average Euclidean nearest neighbor distance (ENN_MN). NP refers to the number of patches in urban land use, ENN_MN is the shortest linear distance between a patch and its same neighbor defined by Euclidean, and PARA_MN is the ratio of the perimeter to the area of the urban patch. NP_MN and ENN_MN can be used to measure the fragmentation of land use patterns, while PARA_MN describes the regularity of urban patches.

Merely describing the various characteristics of the patch is not enough to verify the accuracy of the simulation. The landscape similarity (S_l) proposed by Chen, Li, Wang, Liu

and Ai [45] can be used to calculate the similarity between simulation and real urban land growth. The specific formula is shown in Equation (18):

$$S_l = 1 - \frac{1}{n}\sum_{i}^{n} \Delta l_i$$
$$\Delta l_i = \frac{|l_{is} - l_{ia}|}{l_{ia}} \times 100\%$$

(22)

4. Results

4.1. Actual Urban Growth Characteristics during the Periods of 1995–2005 and 2005–2015

We first reclassified the land use data in the study area and extracted the land use in two periods for superimposition (1995–2005 and 2005–2015). Due to the study of urban land use growth, we regard the water area as the land use type as unchanged, so it is the water area in early 1995. Then we identified the spatial distribution and growth types of newly added urban land (Figure 6). As mentioned earlier, the change in water area was considered in this study to be negligible, and the water area was considered to be a constant. The urban land growth of Wuhan dramatically changed during the two periods. In 1995, Wuhan's non-urban land made up 76.4% of the total, and by 2005, this had decreased to 75.4%. During this period, the urban land increased from 310.36 km^2 to 371.2 km^2. However, from 2005 to 2015, the urban land use increased significantly, to 508.86 km^2. The red and pink areas mainly appeared near the existing urban land. In addition, the urban growth types from 1995 to 2015 appeared relatively consistent, mainly including infilling, edge-expansion and distant-leap types. In the first period (1995–2005), many urban patches of edge-expansion type were found in the existing urban land and few urban patches of distant-leap type appeared around the third ring. In the second period (2005–2015), many urban patches of infilling type appeared near Wujiashan and Jinyinhu, and the urban patches of distant-leap type were found in existing yellow zones. However, the patches of edge-expansion type were decreasing. Consequently, the urban land growth was not only concentrated in the central area, but it also showed a certain range of urban land growth on the periphery of the central area.
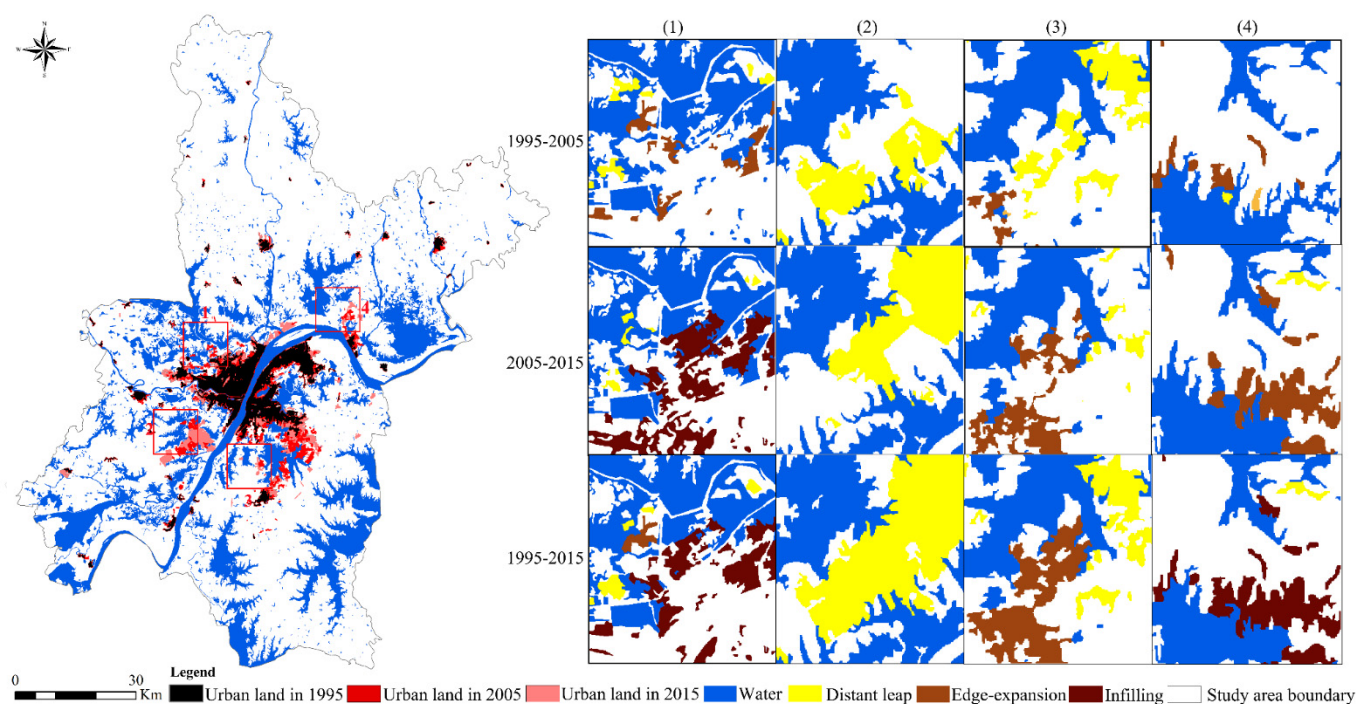

Figure 6. Actual urban growth characteristics of Wuhan in 1995–2015: Urban land area change in 1995–2005 and 2005–2015 (**Left**) and urban land growth types (**Right**): (**1**) Songjiagang and Jinyintan, (**2**) Changfu, (**3**) the left of Zhifang, (**4**) Yangluo.

4.2. Optimized Parameters of Driving Factors in Six Methods

In this study, the driving factors were the distances to national road, highway, provincial road, railway, and country road, plus POP, DEM, and GDP, calculated by the Euclidean distances (Figure 7). Then, the training sample points of the urban grid cells and non-urban grid cells were used to establish a spatial link with the driving factors. Thirdly, these points with other constraint factors were used to calibrate the CA transition rules for 1995 to 2005 by the AFSA algorithm and the other methods.
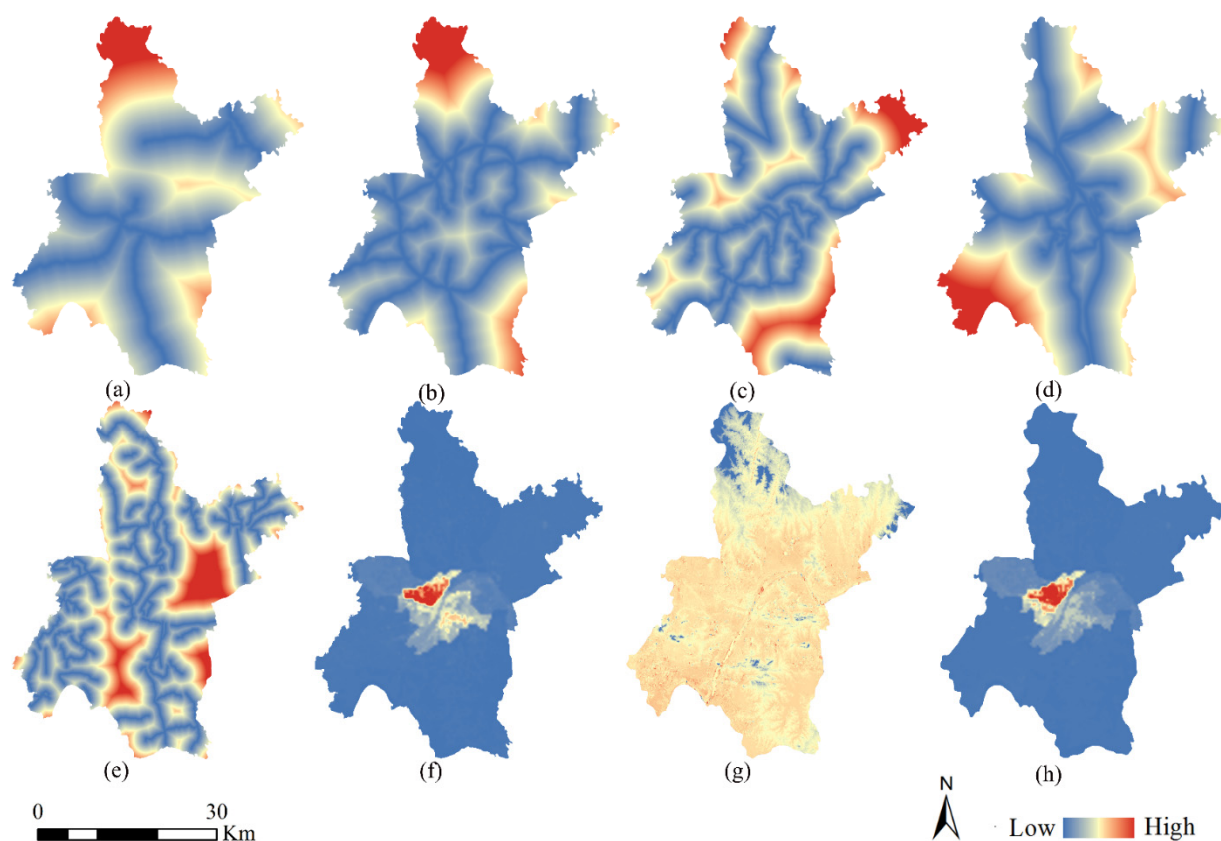

Figure 7. Graphs depicting the spatial variables: (**a**) *D-nat*; (**b**) *D-hig*; (**c**) *D-pro*; (**d**) *D-rai*; (**e**) *D-cou*; (**f**) *POP*; (**g**) *DEM*; (**h**) *GDP*.

We conducted the experiments on a computer with an AMD Ryzen i5-4460 CPU@ 2.30 Hz, 8.00 GB memory and Windows 7. In the MATLAB R2014a environment, the optimized AFSA code, as discussed in attachment materials, was run to obtain the optimal weights of the driving factors, after a number of experiments. The initial "vision" value was Xmax/2 (where Xmax denotes the maximum visual search range); the dynamic step size was visual/8; the minimum value of visual was 0.2; the maximum value was 10; and the minimum and maximum values of the step size were 0.02 and 10, respectively. MAXGEN represents the maximum number of iterations. The parameter weight combination value (Table 3) is mostly negative.

In this study, the swarm intelligence algorithms and the BLR method were chosen to establish a model comparison. The swarm intelligence approach has a wide range of applications, robust design, and greater application value. The BLR method is an empirical model that requires a linearly independent variable, and is typically used to define the relationship (0 or 1) between one or more driving factors and the actual binary reality. The weight values of the CA parameters obtained using the various models are listed in Table 4. Since the urban growth area is negatively correlated with distance, the distance should be negative. Among the six models, however, only the GA-CA model and the AFSA-CA model fit the facts. In

addition, the POP variable should be positively correlated with the urban growth, but the parameter value of the GA-CA model is −15.5409.

Table 4. The parameters of the cellular automaton (CA) models.

Variable	BLR-CA	ACO	BBO-CA	PSO-CA	GA-CA	AFSA-CA
D-nat	−4.3100	−10.1042	−5.2933	−3.9468	−16.4928	−4.9734
D-hig	−5.4880	−0.5539	−8.2734	−4.1205	−2.1272	−1.1546
D-pro	−4.6970	1.9882	4.0829	1.0876	−3.2782	−19.5246
D-rai	−10.238	−3.1680	−13.6067	−1.5529	−15.2515	−2.1672
D-cou	0.9850	6.0789	−6.9345	8.4651	−18.3324	−1.2427
POP	1.6110	−3.1961	12.7117	9.6026	−15.5409	1.1224
DEM	−7.4510	9.0272	14.4608	15.9637	−15.0850	1.4027
GDP	0.0450	−2.2814	−8.2408	16.8328	−4.7409	−17.7256
Constant	−1.4580	−4.1444	−14.431	−4.1565	−4.1230	−0.3092

4.3. Simulated Results of Six Optimized CA Models

After acquiring the transition probability matrix using ArcGIS, the results were input into the CA model to simulate the urban land-use change of Wuhan from 2005 to 2015. The urban land growth simulation experiments were implemented in Matlab 2014a. According to the previous literature and constant trial and error experiments, we selected the 7×7 extended Moore neighborhood and 2 as a parameter that controls the degree of *Rand* [18]. After obtaining the conversion probability of each cell according to formula 5 mentioned in Section 3.1, the increased urban land area of Wuhan was regarded as the end condition of CA models. By dividing the total number of new increased urban land cells by the number of iterations, the transformed number of cells in each iteration can be calculated [46]. The number of iterations in our study was set to 20 as the ten-time span.

The results of the AFSA-CA model simulation are shown in Figure 8. This shows the actual urban land use and the AFSA-CA model simulation for 2015. The simulation image on the right shows a pattern of agglomerative growth in the central area of Wuhan, in addition to a point-like expansion in the south and north of the edge of the central area, while the farther area outside the central area shows a leap-forward expansion form. This is highly consistent with Wuhan's actual expansion. To better verify the accuracy of the simulation, the Kappa coefficient, FoM, UA, and TA were compared, and the results are shown in Table 4. In the Kappa coefficient calculation, a value higher than 0.6 indicates strong consistency, and subsequent lesser values indicate medium or weak consistency. The AFSA-CA model in Kappa coefficient of 0.7948 represents a strong agreement between the actual value and the simulated value. Based on the above conclusions, it can be said that the AFSA-CA model is able to obtain satisfactory modeling parameters for the calibration of the urban growth in Wuhan. The value of FoM is defined as the ratio between the observed value and the correct region of the predicted value, ranging from 0 to 1, where the higher the score, the better the simulation results of the urban land-use change model. Here, the AFSA-CA model obtains a FoM value that is 0.02 higher than the result of the GA-CA model. At the same time, the other two indicators—UA and TA—can also be used to indicate the fit of the simulation model. The UA of the AFSA-CA model is equal to 0.8157, indicating that the urban area is close to the actual value. In addition, the TA is equal to 0.9771, and the analog error is 0.0229, indicating a very high simulation success rate.

The simulation results of the five comparison models shown in Figure 8 display different degrees of urban land-use growth. The PSO-CA model shows the most obvious difference, and the simulation results show excessive dot-like expansion, i.e., the north of Wuhan appears expanded as dotted lines, which is inconsistent with reality. The map of the BLR-CA model shows a large increase in the dotted pattern for the south of Wuhan. The other models also show different degrees of expansion. As mentioned in Section 3.2, AFSA has the advantages of a fast convergence speed, insensitivity to the initial values, strong adaptability, and strong fault tolerance. In contrast, BLR is a static model with

serious defects, because variables driving changes of urban growth are non-linear rather than linear relationships. Therefore, the AFSA-CA model is superior to the GA-CA model, and the GA-CA model is superior to all the other models.
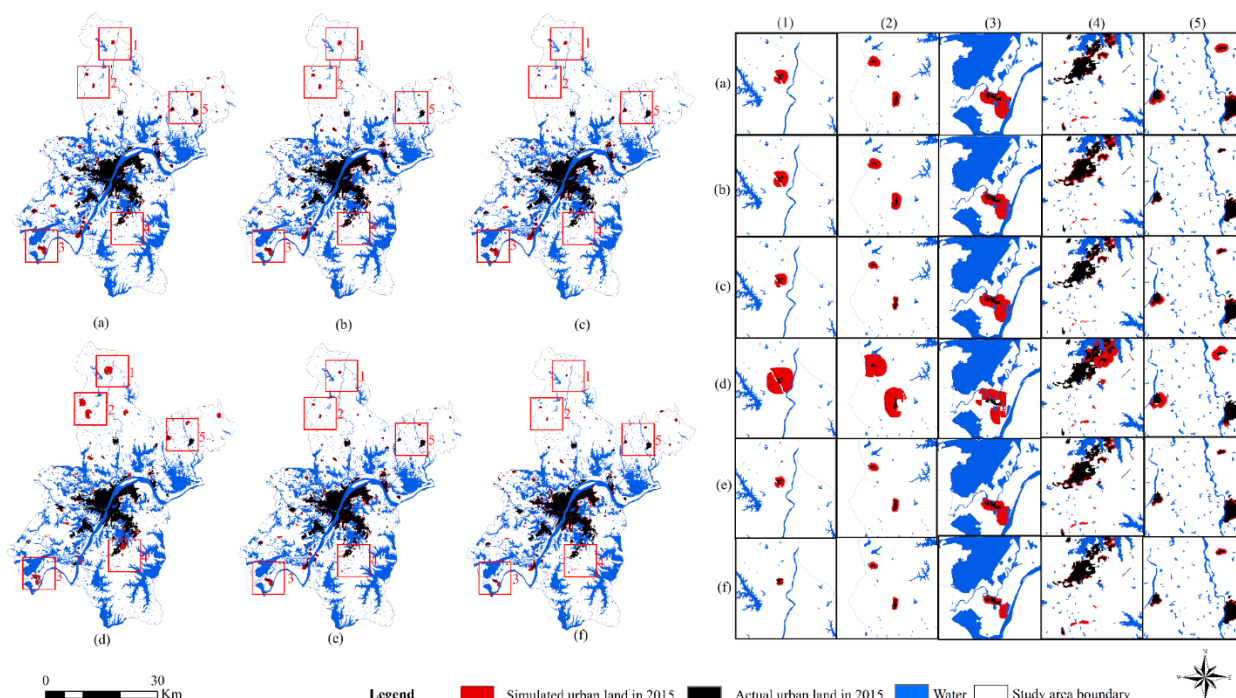

Figure 8. Urban land-use change prediction for Wuhan in 2015, based on the different CA models: (**a**) BLR-CA; (**b**) ACO-CA; (**c**) BBO-CA; (**d**) PSO-CA; (**e**) GA-CA; (**f**) AFSA-CA.

The accuracy of the five models is represented by the verified Kappa coefficients, FoM, UA, and TA (Table 5). The Kappa coefficient of the GA-CA model is verified to be 0.7777, which is 0.2 times higher than the BLA-CA value, and is higher than the values of the other models. The parameter analysis and simulation analysis results are also consistent. In addition, the Kappa coefficient of PSO-CA is as low as 0.7168, and the UA is only 0.7416, further affirming the precision of the previous analysis. However, compared to the AFSA-CA model, the simulation accuracy of the GA-CA model falls short. For example, the TA value of AFSA-CA reaches 0.9771, but the TA value of GA-CA value is only 0.9753.

Table 5. Validation of the urban land-use change prediction for Wuhan based on the different CA models.

Variable	BLR-CA	ACO-CA	BBO-CA	PSO-CA	GA-CA	AFSA-CA
Kappa	0.7507	0.7701	0.7692	0.7168	0.7777	0.7948
FoM	0.6393	0.6698	0.6519	0.5976	0.6748	0.6975
UA	0.7738	0.7923	0.7914	0.7416	0.7996	0.8157
TA	0.9722	0.9744	0.9743	0.9685	0.9753	0.9771

We use four landscape metrics (NP, PARA_MN, ENN_MN and a_l) to compare the simulated results in six CA models as shown in Table 6. As seen from the Table 6, AFSA-CA has a better performance in landscape similarity than other five models. The landscape similarity between the AFSA-CA simulated results and the actual values in 2015 is 85.91%, which is 5.82–16.25% higher than other five simulated results. The NP value of AFSA-CA is closer to the actual, with a difference of merely 318, while the worst result of the NP value is a difference of 642, more than twice. Although the simulated results for GA-CA performed well, the proposed model still maintained the better satisfactory values in the

urban landscape. Consequently, these landscape metrics results showed that AFSA-CA in calibrating the parameters of CA achieves the desired goal.

Table 6. Comparison of actual and simulated various results of landscape metrics.

Variable	NP	PARA_MN	ENN_MN	S_I
Actual (2015)	1645	242.4455	440.5482	——
Simulated (BLR-CA)	1012	170.6062	521.4226	71.18%
Simulated (ACO-CA)	1203	195.3048	509.1447	79.37%
Simulated (BBO-CA)	1108	184.6976	515.1334	75.54%
Simulated (PSO-CA)	1003	173.1665	543.6949	69.66%
Simulated (GA-CA)	1249	289.5169	512.1332	80.09%
Simulated(AFSA-CA)	1327	266.3229	498.2074	85.91%

5. Discussion and Implications

5.1. Effects of Differences Models on Urban Growth Simulation

The AFSA-CA model outperformed the other five models in simulation of the urban growth in Wuhan under the same land use data and driving factors data. The Kappa value of AFSA-CA model is the highest at 0.7948, with 0.0816 higher than the lowest one (PSO-CA), while the UA and TA of AFSA-CA model are 0.8157 and 0.9771, respectively. PSO is likely to fall into local extreme, and its optimization accuracy is poor, whereas AFSA only uses the function value of the target problem, and has a certain adaptive ability to the search space [39,47]. The second highest of Kappa value is GA-CA model, while its TA reaches to 0.9753. Although the crossover and mutation selection probability of GA directly affects the convergence of the algorithm [48], resulting in the simulation results of GA-CA model are the closest to AFSA-CA, the urban land growth area in the east-west direction of Wuhan is quite different from the actual situation. The other three models (BLR-CA, ACO-CA and BBO-CA) see a relatively low in the validation indexes, such as the Kappa value of these models being below 0.77. BLR obtained higher receiver operating characteristic curve values [49], but the non-linear relationship of the drivers of urban growth made the LR-CA model show a weak performance [50]. ACO and AFSA algorithms both belong to the swarm intelligence algorithms, the "ants" of ACO have no vision to help them find the best food source [51]. BBO performs good information sharing characteristic, but the traditional method of gene migration is single. The urban land growth simulation has constraints, and the migration and mutation operators must be adjusted accordingly during the simulation process [20]. Consequently, AFSA is not affected by the initial parameter setting, and is one of the most effective algorithms for solving nonlinear optimization problems compared with other algorithms.

5.2. Future Scenario Simulation for Wuhan in 2025 and 2035

Urban land simulation models are conducive to formulating reasonable sustainable development strategies and helping governments and planners [52]. The weight parameter corresponding to each spatial variable in the CA model, which is directly determined with the naked eye or subjectively, is time-consuming [11,53]. Based on the results, it was apparent that AFSA-CA was the most suitable simulation model for the urban growth of the study area. Hence, we adopted three future scenarios based on previous research: (1) natural urban land growth without any restrictions (NULG), (2) sustainable urban land growth with cropland protection and ecological security (SULG) and (3) economic urban land growth with sustainable development and economic development in the core area (EULG) [10,54].

In the first urban land growth scenario, the total conversion area of urban land from non-urban land in 2025 and 2035 was based on an unrestricted AFSA-CA model to predict. According to China's ecological control plan and farmland protection policy, the Municipal Government of Wuhan implemented protection of ecological land and farmland, the conversion for which land-use types is not allowed. The SULG scenario limited the

conversion of cropland, forest, grassland into urban land. However, these strict restrictions for land conversion are harmful to urban development. Combined with the comprehensive supporting facilities in the core area, it is more realistic to release control over the core area. Therefore, the EULG scenario of this study was based on SULG, which only controlled the conversion of non-urban land in areas far from the central area to urban land in the process of urban growth.

Figure 9 shows the predicted results of 2025 and 2035 under three proposed future scenarios. The urban development of Wuhan follows a multi-center structure developmental model. The urban land area of Wuhan is predicted to reach 137.65 km² in the 10 years from 2015, accounting for nearly 8% of the total area, and representing an increase of about 1.6%. Conversely, non-urban land is predicted to reduce to 607.19 km². The urban land in Wuhan is expected to continue expanding up to 2035, and the non-urban land area is predicted to decrease. The urban land area in Wuhan is predicted to reach 762.23 km², accounting for nearly 9% of the total land area, and the non-urban land area is expected to decrease to 5945.16 km², with the water area remaining largely unchanged. This growth is in line with Wuhan's overall urban plan. Therefore, a single-center structure results in a "siphon effect" for the central city, with a concentration of elements such as technology and capital. It can also result in a highly concentrated population density and a high density of buildings.
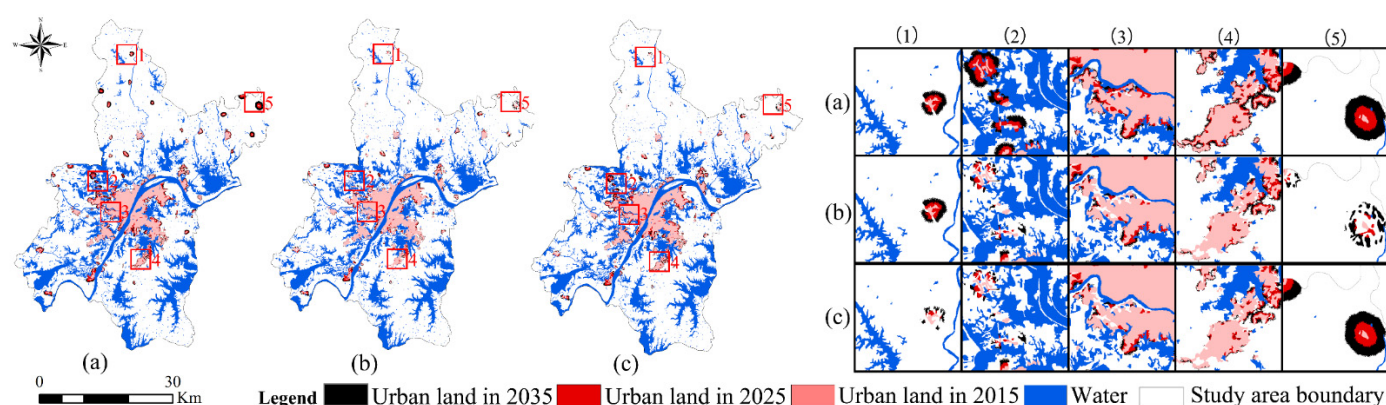

Figure 9. Simulated urban land growth of Wuhan under different urban land growth scenarios: (**a**) NULG, (**b**) SULG and (**c**) EULG in 2025 and 2035.

However, the newly developed centers have different strengths and development orders, and the development is not parallel development. The urban land growth in Wuhan shows significant spatial heterogeneity in the different regions. The pink area in the Figure 9 which is the existing urban land before 2015 occupies a large space, while the red and black area mostly appear in the new district centers. Compared with the NULG scenario, the urban land distribution in the SULG scenario is most obvious in Jiaji Yao and Gu Xu in the north direction, while the conversion restriction in the south direction is not much different from the urban land distribution in the NULG scenario. Under the EULG scenario, urban land in the core area grows unrestrictedly, and the growth type is mainly infilling. Consequently, the predicted quantity and location results of potential increased urban land in 2025 and 2035 under three different scenarios can be helpful for future urban planning.

Based on the results of the AFSA-CA simulation model for 2025 and 2035, the urban development of Wuhan is predicted to be no longer a single center, but will instead incorporate the emergence of a certain proportion of development in each new deputy center, town center, etc. The urbanization process of Wuhan will experience different spatial growth patterns in two periods. In the early stage, the urban land growth in remote areas will still account for the main part of the newly added urban area. Later, the growth area of remote areas gradually will decrease, and the urban land growth form will enter a very mature stage [55]. In addition, the spatial development pattern of Wuhan in the future will appear a form of multi-centered urban development [56].

In the NULG scenario, the urban land use in the core area will decrease, while the deputy centers and new town centers will increase. However, disorderly urban land use growth is not in line with China's sustainable development strategy [54]. In the SULG scenario, the conversion of cultivated land and ecological land into urban land is prohibited. Figure 9b shows that the growth of urban land in remote areas has decreased significantly. At the same time, the growth of urban land in the core area is directly restricted. In order to adapt to the future social-economic development, the morphological characteristics of urban development tend to be increasingly based on multi-center development [10,57,58]. The EULG scenario, and the urban development form appears to be more compact [55]. The formulation of specific urban planning should be flexible accordingly [59].

5.3. Role of Urban Growth Simulation for Smart City

Urban sustainable development and management is one of the 17 Sustainable Development Goals [60]. The smart city is essential to enhance the urban planning and offer more comfortable human settlements. The contradiction between the limited urban land area and the needs of construction land use in highly competitive economic context become increasingly intensified with different levels of land degeneration, environmental pollution and a drastic population growth. Based on our results, the future urban growth pattern of Wuhan should be based on placing mainly the central activity area, then developing the city sub-center, new city center and main town center.

Regarding urban planning of Wuhan, it is in line with development of other big cities in China. Constructing a polycentric urban structure in Wuhan is highly important to reduce the negative impacts of high density in the city center [61]. Urban planning has gradually popularized since 1980s. By 1990, the growth of urban space along the axis began to weaken, and then leapfrog development became the focus of urban development [62]. Since urban land in Wuhan does not meet the needs of rapid urban development, resulting in urban expansion of the entire city, urban planning is adjusted accordingly [63]. In the simulation, the central area expansion denotes mainly concentrated growth, and the point-like growth of the edge area began to appear in the later stage. Therefore, the formulation of specific urban planning should be flexible [64].

Such simulation help explore the relative impacts of variables on urban land use changes and the characteristics of urban growth pattern [65]. Moreover, artificial intelligence algorithm provides explicit information on potentials of urban areas. Projecting the potential urban areas under different scenarios can make a comparison between the modelled results and the plans, and provide references about whether relevant policies and plans need to be adjusted with authorities and planner researchers. It is a comprehensive and scientific method to support urban growth patterns.

6. Conclusions

The AFSA-CA model proposed in this study incorporates historical characteristics of urban growth, driving factors and a novel algorithm, for improving the prediction accuracy of urban growth processes. Six different methods from traditional to intelligent algorithm technology were combined with the CA model to explore the characteristics of urban growth, while a series of measures were applied for the verification, including the Kappa coefficient, FoM, UA, TA, and landscape indicators. Based on the confusion matrix calculation and other verification indexes, the range of the total precision difference between BLR-CA and AFSA-CA, and BLR-CA and GA-CA, was found to be 5% and 3%, respectively. The verification results showed that the AFSA-CA model performed better than the other five models, due to an optimal advantage for solving nonlinear optimization problems, which AFSA is not affected by the initial parameter setting. Furthermore, we projected the potential patterns of urban growth under different scenarios in the 20 years to come, before understanding historical land use characteristics in past 20 years, the political restrictions on cultivated land and ecological land, and actual local development conditions. We found that the potentials of urban growth in Wuhan for 2025 and 2035 under three

scenarios (NULG, SULG, and EULG) focus mainly on existing urban land and some new town centers based on AFSA-CA urban growth simulation model.

The smart city refers to the use of information and communication technology to analyze the key information of the urban system, and promote the harmonious and sustainable development of the city. Only cities that integrate these data and science and technology to improve urban efficiency, equity, sustainability, and quality of life can be called smart cities. The Ministry of Science and Technology of China recognized Wuhan as the first batch of innovative pilot cities and launched a pilot smart city construction. The national and local authorities have introduced relevant plans integrating the planning concepts and technological advantages at domestic and international first-class institutions for smart city construction of Wuhan. In accordance with the foundational principle of people's livelihood first, priority will be given to projects that are closely related to people's livelihood for first demonstration construction. Through management, control and optimization, the infrastructure of a smart city is associated with its operational functions and planning. As cities develop smarter, long-term changing information can provide new immediacy for the construction of urban simulation models. Accordingly, simulating different models of future cities can better understand the complex science of cities.

According our results, we have some suggestions for the urban areas planning in Wuhan: firstly, it is necessary to consider the development of town centers because the central area has been saturated in urban land use; secondly, intensive developing in the central area is not suitable environment for dwellers, so increasing traffic networks for remote areas are inevitable; finally, it is necessary to design different plans under various scenarios to cater for the needs of future development. Although the prediction may dissatisfy the actual urban land needs due to emergencies (such as COVID-19), a more precise simulation can determine the potential increase area and quantity of urban land, providing a basis to judge the layout of urban land use for urban planners. However, whether AFSA is able to avoid radically is still a matter within scientific communities, despite of excellent performance in the tolerance of local extrema. Under the limitations of experimental data and environment, this study focuses on urban growth simulation of a local scale by six different integrated models, where the characteristics of urban growth patterns differ from geographic and economic context. Henceforth, further research is to apply this research method to other regions and countries, to enlarge the practicality of the method.

Author Contributions: Conceptualization, G.X.; Data curation, F.X.; Investigation, F.X.; Visualization, G.X.; Writing-review & editing, X.H. All authors have read and agreed to the published version of the manuscript.

Conflicts of Interest: The authors declare no conflict of interest.

Abbreviations

CA	the cellular automaton
BLR	binary logistic regression
GAs	genetic algorithms
ACOs	ant colony algorithms
PSO	particle swarm optimization
BBO	biogeography-based optimization
AFSA	artificial fish swarm algorithm
Neib	neighborhoods

Suit	constraints
Rand	random factors
UA	urban accuracy
TA	total accuracy
NP	the number of urban patches
PARA_MN	average perimeter ratio
ENN_MN	average Euclidean nearest neighbor distance
POP	population
DEM	digital elevation model
GDP	gross domestic product
LUD_1	Land-use in 1995
LUD_2	Land-use in 2005
LUD_3	Land-use in 2015
D-nat	Distance to national road
D-hig	Distance to highway
D-pro	Distance to provincial road
D-rai	Distance to railway
D-cou	Distance to country road
NEI	Neighhood cell
NULG	natural urban land growth without any restrictions
SULG	sustainable urban land growth with cropland protection and ecological security
EULG	economic urban land growth with sustainable development and economic development in the core area

References

1. United Nations. *World Urbanization Prospects: The 2018 Revision*; United Nations Department of Economic and Social Affairs: New York, NY, USA, 2019.
2. Zhang, W.; Li, W.; Zhang, C.; Hanink, D.M.; Liu, Y.; Zhai, R. Analyzing horizontal and vertical urban expansions in three East Asian megacities with the SS-coMCRF model. *Landsc. Urban Plan.* **2018**, *177*, 114–127. [CrossRef]
3. Chuang, U.; Cho, J.; Yun, J. Urbanization effect on the observed change in mean monthly temperatures between 1951–1980 and 1971–2000 in Korea. *Clim. Chang.* **2011**, *66*, 127–136. [CrossRef]
4. Lee, D.; Choe, H. Estimating the Impacts of Urban Expansion on Landscape Ecology: Forestland Perspective in the Greater Seoul Metropolitan Area. *J. Urban Plan. Dev.* **2011**, *137*, 425–437. [CrossRef]
5. Zhou, Y.; Huang, B.; Wang, J.; Chen, B.; Kong, H.; Norford, L. Climate-Conscious Urban Growth Mitigates Urban Warming: Evidence from Shenzhen, China. *Environ. Sci. Technol.* **2019**. [CrossRef]
6. Camero, A.; Alba, E. Smart City and information technology: A review. *Cities* **2019**, *93*, 84–94. [CrossRef]
7. Clarke, K.C.; Hoppen, S. A self-modifying cellular automaton model of historical urbanization in the San Francisco Bay area. *Environ. Plan.* **1997**, *24*, 247–261. [CrossRef]
8. Xu, T.; Gao, J.; Coco, G.; Wang, S. Urban expansion in Auckland, New Zealand: A GIS simulation via an intelligent self-adapting multiscale agent-based model. *Int. J. Geogr. Inf. Sci.* **2020**, *34*, 1–24. [CrossRef]
9. Chen, G.; Li, X.; Liu, X.; Chen, Y.; Liang, X.; Leng, J.; Xu, X.; Liao, W.; Qiu, Y.a.; Wu, Q.; et al. Global projections of future urban land expansion under shared socioeconomic pathways. *Nat. Commun.* **2020**, *11*, 1–12. [CrossRef]
10. Yang, Y.; Bao, W.; Liu, Y. Scenario simulation of land system change in the Beijing-Tianjin-Hebei region. *Land Use Policy* **2020**, *96*, 104677. [CrossRef]
11. He, J.; Li, X.; Yao, Y.; Hong, Y.; Jinbao, Z. Mining transition rules of cellular automata for simulating urban expansion by using the deep learning techniques. *Int. J. Geogr. Inf. Sci.* **2018**, *32*, 2076–2097. [CrossRef]
12. Wu, F.; Webster, C.J. Simulation of Land Development through the Integration of Cellular Automata and Multicriteria Evaluation. *Environ. Plann. B Plan. Des.* **1998**, *25*, 103–126. [CrossRef]
13. Naghibi, F.; Delavar, M.R.; Pijanowski, B. Urban Growth Modeling Using Cellular Automata with Multi-Temporal Remote Sensing Images Calibrated by the Artificial Bee Colony Optimization Algorithm. *Sensors* **2016**, *16*, 2122. [CrossRef]
14. Naghibi, F.; Delavar, M. Discovery of Transition Rules for Cellular Automata Using Artificial Bee Colony and Particle Swarm Optimization Algorithms in Urban Growth Modeling. *ISPRS Int. J. Geo-Inf.* **2016**, *5*, 241. [CrossRef]
15. Wang, H.; Xia, C.; Zhang, A.; Zhang, W. Calibrating urban expansion cellular automata using biogeography based optimization. *Geomat. Inf. Sci. Wuhan Univ.* **2017**, *42*, 1323–1329.
16. Al-Kofahi, S.D.; Hammouri, N.; Sawalhah, M.N.; Al-Hammouri, A.A.; Aukour, F.J. Assessment of the urban sprawl on agriculture lands of two major municipalities in Jordan using supervised classification techniques. *Arab. J. Geosci.* **2018**, *11*, 45. [CrossRef]
17. Rienow, A.; Goetzke, R. Supporting SLEUTH—Enhancing a cellular automaton with support vector machines for urban growth modeling. *Comput. Environ. Urban Syst.* **2015**, *49*, 66–81. [CrossRef]

18. Wu, H.; Li, Z.; Clarke, K.C.; Shi, W.; Fang, L.; Lin, A.; Zhou, J. Examining the sensitivity of spatial scale in cellular automata Markov chain simulation of land use change. *Int. J. Geogr. Inf. Sci.* **2019**, *33*, 1040–1061. [CrossRef]
19. Hagenauer, J.; Omrani, H.; Helbich, M. Assessing the performance of 38 machine learning models: The case of land consumption rates in Bavaria, Germany. *Int. J. Geogr. Inf. Sci.* **2019**, *33*, 1399–1419. [CrossRef]
20. Farswan, P.; Bansal, J.C. Fireworks-inspired biogeography-based optimization. *Soft Comput.* **2018**, *23*, 7091–7115. [CrossRef]
21. Li, X.; Lin, J.; Chen, Y.; Liu, X.; Ai, B. Calibrating cellular automata based on landscape metrics by using genetic algorithms. *Int. J. Geogr. Inf. Sci.* **2013**, *27*, 594–613. [CrossRef]
22. Yazdani, D.; Nasiri, B.; Sepas-Moghaddam, A.; Meybodi, M.; Akbarzadeh-Totonchi, M. mNAFSA: A novel approach for optimization in dynamic environments with global changes. *Swarm Evol. Comput.* **2014**, *18*, 38–53. [CrossRef]
23. Li, X.L. An Optimi zing Method Based on Autonomous Animats: Fish-swarm Algorithm. *Syst. Eng. Theory Pract.* **2002**, *22*, 32–38.
24. Li, X.-L.; Xue, Y.-C.; Lu, F.; Tian, G.-H. Parameter estimation method based-on artificial fish school algorithm. *J. Shandong Univ.* **2004**, *34*, 84–87.
25. Neshat, M.; Sepidnam, G.; Sargolzaei, M.; Toosi, A.N. Artificial fish swarm algorithm: A survey of the state-of-the-art, hybridization, combinatorial and indicative applications. *Artif. Intell. Rev.* **2012**, *42*, 965–997. [CrossRef]
26. Gao, Y.; Guan, L.; Wang, T.; Sun, Y. A novel artificial fish swarm algorithm for recalibration of fiber optic gyroscope error parameters. *Sensors* **2015**, *15*, 10547–10568. [CrossRef]
27. Chen, W.; Feng, Y.-Z.; Jia, G.-F.; Zhao, H.-T. Application of Artificial Fish Swarm Algorithm for Synchronous Selection of Wavelengths and Spectral Pretreatment Methods in Spectrometric Analysis of Beef Adulteration. *Food Anal. Methods* **2018**, *11*, 2229–2236. [CrossRef]
28. Shao, H.; Jiang, H.; Zhao, H.; Wang, F. A novel deep autoencoder feature learning method for rotating machinery fault diagnosis. *Mech. Syst. Signal Process.* **2017**, *95*, 187–204. [CrossRef]
29. Zhao, W.; Du, C.; Jiang, S. An adaptive multiscale approach for identifying multiple flaws based on XFEM and a discrete artificial fish swarm algorithm. *Comput. Methods Appl. Mech. Eng.* **2018**, *339*, 341–357. [CrossRef]
30. Azad, M.A.K.; Rocha, A.M.A.C.; Fernandes, E.M.G.P. Improved binary artificial fish swarm algorithm for the 0–1 multidimensional knapsack problems. *Swarm Evol. Comput.* **2014**, *14*, 66–75. [CrossRef]
31. Zhang, Z.; Wang, K.; Zhu, L.; Wang, Y. A Pareto improved artificial fish swarm algorithm for solving a multi-objective fuzzy disassembly line balancing problem. *Expert Syst. Appl.* **2017**, *86*, 165–176. [CrossRef]
32. Liu, X.; Liu, H.; Yang, J.; Litak, G.; Cheng, G.; Han, S. Improving the bearing fault diagnosis efficiency by the adaptive stochastic resonance in a new nonlinear system. *Mech. Syst. Signal Process.* **2017**, *96*, 58–76. [CrossRef]
33. He, Q.; Hu, X.; Ren, H.; Zhang, H. A novel artificial fish swarm algorithm for solving large-scale reliability-redundancy application problem. *ISA Trans.* **2015**, *59*, 105–113. [CrossRef]
34. Luo, T.; Tan, R.; Kong, X.; Zhou, J. Analysis of the Driving Forces of Urban Expansion Based on a Modified Logistic Regression Model: A Case Study of Wuhan City, Central China. *Sustainability* **2019**, *11*, 2207. [CrossRef]
35. Chen, W.; Zhao, H.; Li, J.; Zhu, L.; Wang, Z.; Zeng, J. Land use transitions and the associated impacts on ecosystem services in the Middle Reaches of the Yangtze River Economic Belt in China based on the geo-informatic Tupu method. *Sci. Total Environ.* **2019**, *701*, 134690. [CrossRef] [PubMed]
36. Feng, Y.; Tong, X. Using exploratory regression to identify optimal driving factors for cellular automaton modeling of land use change. *Environ. Monit. Assess.* **2017**, *189*, 515. [CrossRef] [PubMed]
37. Zhang, B.; Wang, H.; He, S.; Xia, C. Analyzing the effects of stochastic perturbation and fuzzy distance transformation on Wuhan urban growth simulation. *Trans. GIS* **2020**, *24*, 1779–1798. [CrossRef]
38. Wu, F. Calibration of stochastic cellular automata: The application to rural-urban land conversions. *Int. J. Geogr. Inf. Sci.* **2002**, *16*, 795–818. [CrossRef]
39. Wang, L.G.; Shi, Q.H.; Hong, Y. Hybrid Optimization Algorithm of PSO and AFSA. *Comput. Eng.* **2010**, *36*, 176–178. [CrossRef]
40. Wu, F. An Experiment on the Generic Polycentricity of Urban Growth in a Cellular Automatic City. *Environ. Plan. B Plan. Des.* **1998**, *25*, 731–752. [CrossRef]
41. Simon, D. Biogeography-Based Optimization. *IEEE Trans. Evol. Comput.* **2008**, *12*, 702–713. [CrossRef]
42. Shan, J.; Alkheder, S.; Wang, J. Cellular automata urban growth model calibration with genetic algorithms. *Photogramm. Eng. Remote Sens.* **2007**, *74*, 1267–1277. [CrossRef]
43. He, Q.; Tan, S.; Yin, C.; Zhou, M. Collaborative optimization of rural residential land consolidation and urban construction land expansion: A case study of Huangpi in Wuhan, China. *Comput. Environ. Urban Syst.* **2019**, *74*, 218–228. [CrossRef]
44. Pontius, R.G.; Boersma, W.; Castella, J.-C.; Clarke, K.; de Nijs, T.; Dietzel, C.; Duan, Z.; Fotsing, E.; Goldstein, N.; Kok, K.; et al. Comparing the input, output, and validation maps for several models of land change. *Ann. Reg. Sci.* **2007**, *42*, 11–37. [CrossRef]
45. Chen, Y.; Li, X.; Wang, S.; Liu, X.; Ai, B. Simulating Urban Form and Energy Consumption in the Pearl River Delta Under Different Development Strategies. *Ann. Assoc. Am. Geogr.* **2013**, *103*, 1567–1585. [CrossRef]
46. Li, X.; Liu, X.; Yu, L. A systematic sensitivity analysis of constrained cellular automata model for urban growth simulation based on different transition rules. *Int. J. Geogr. Inf. Sci.* **2014**, *28*, 1317–1335. [CrossRef]
47. Jiang, C.; Wan, L.; Sun, Y.; Li, Y. The Application of PSO-AFSA Method in Parameter Optimization for Underactuated Autonomous Underwater Vehicle Control. *Math. Probl. Eng. Eng.* **2017**, *2017*, 1–14. [CrossRef]

48. Ma, C.; He, R. Green wave traffic control system optimization based on adaptive genetic-artificial fish swarm algorithm. *Neural Comput. Appl.* **2015**, *31*, 2073–2083. [CrossRef]

49. Park, S.; Jeon, S.; Kim, S.; Choi, C. Prediction and comparison of urban growth by land suitability index mapping using GIS and RS in South Korea. *Landsc. Urban Plan.* **2011**, *99*, 104–114. [CrossRef]

50. Mustafa, A.; Van Rompaey, A.; Cools, M.; Saadi, I.; Teller, J. Addressing the determinants of built-up expansion and densification processes at the regional scale. *Urban Stud.* **2018**, *55*, 3279–3298. [CrossRef]

51. Blum, C.; Dorigo, M. The Hyper-Cube Framework for Ant Colony Optimization. *IEEE Trans. Syst. Man Cybern. Part B* **2004**, *34*, 1161–1172. [CrossRef] [PubMed]

52. Li, X.; Yeh, A.G.-O. Modelling sustainable urban development by the integration of constrained cellular automata and GIS. *Int. J. Geogr. Inf. Sci.* **2000**, *14*, 131–152. [CrossRef]

53. White, R. Cellular automata and fractal urban form: A cellular modelling approach to the evolution of urban land-use patterns. *Environ. Plan. A Plan. Des.* **1993**, *25*, 1175–1199. [CrossRef]

54. Yao, Y.; Liu, X.; Li, X.; Liu, P.; Hong, Y.; Zhang, Y.; Mai, K. Simulating urban land-use changes at a large scale by integrating dynamic land parcel subdivision and vector-based cellular automata. *Int. J. Geogr. Inf. Sci.* **2017**, *31*, 2452–2479. [CrossRef]

55. He, Q.; Liu, Y.; Zeng, C.; Chaohui, Y.; Tan, R. Simultaneously simulate vertical and horizontal expansions of a future urban landscape: A case study in Wuhan, Central China. *Int. J. Geogr. Inf. Sci.* **2017**, *31*, 1907–1928. [CrossRef]

56. Ke, X.; Zheng, W.; Zhou, T.; Liu, X. A CA-based land system change model: LANDSCAPE. *Int. J. Geogr. Inf. Sci.* **2017**, *31*, 1798–1817. [CrossRef]

57. Xia, C.; Zhang, A.; Wang, H.; Zhang, B. Modeling urban growth in a metropolitan area based on bidirectional flows, an improved gravitational field model, and partitioned cellular automata. *Int. J. Geogr. Inf. Sci.* **2019**, *33*, 877–899. [CrossRef]

58. Yang, J.; Gakenheimer, R. Assessing the transportation consequences of land use transformation in urban China. *Habitat Int.* **2007**, *31*, 345–353. [CrossRef]

59. Wang, M.; Krstikj, A.; Koura, H. Effects of urban planning on urban expansion control in Yinchuan City, Western China. *Habitat Int.* **2017**, *64*, 85–97. [CrossRef]

60. Chai, B.; Seto, K.C. Conceptualizing and characterizing micro-urbanization: A new perspective applied to Africa. *Landsc. Urban Plan.* **2019**, *190*, 103595. [CrossRef]

61. Yuan, M.; Huang, Y.; Shen, H.; Li, T. Effects of urban form on haze pollution in China: Spatial regression analysis based on PM2.5 remote sensing data. *Appl. Geogr.* **2018**, *98*, 215–223. [CrossRef]

62. Luo, M. Motivity of Spatial Urban Expansion by Cellular Automata Model —Taking Analysis of Wuhan Spatial Urban Expansion as an Example. *Geomat. Inf. Sci. Wuhan Univ.* **2005**, *30*, 52–55. [CrossRef]

63. Yu, D. Self-organization characteristics of urban extension and the planning effect evaluation A case study of Beijing. *Geogr. Res.* **2016**, *35*, 353–362. [CrossRef]

64. Wang, T.; Han, Q.; de Vries, B. A semi-automatic neighborhood rule discovery approach. *Appl. Geogr.* **2017**, *88*, 73–83. [CrossRef]

65. Xu, T.; Gao, J.; Li, Y. Machine learning-assisted evaluation of land use policies and plans in a rapidly urbanizing district in Chongqing, China. *Land Use Policy* **2019**, *87*, 104030. [CrossRef]